Volume 4, Issue 3, 2026

Frontier in Medical & Health Research

ISSN: (e) 3007-1607 (p) 3007-1593

PHARMACOLOGICAL EVALUATION OF METHYSTICIN-LOADED NANOPARTICLES IN $AlCl_3$ INDUCED ALZHEIMER'S DISEASE

Muhammad Siraj[*1], Naseer Ahmad[2], Rubia Anwer[3], Ch Bakhtawar Khan[4], Abida Shamim[3], Muhammad Azlan Shah[5], Syed Asim Shah[6], Iffat Ullah[7], Muhammad Faheem[8]

[1]*Department of Pharmacy, Abbottabad University of Science and Technology*
[2]*Canterbury Christ Church University United Kingdom*
[3]*Faculty of Pharmacy, IBADAT International University Islamabad, Pakistan*
[4]*Department of Pharmacy, University of Chakwal, Chakwal Campus*
[5]*Department of Pharmacy, Sarhad University of Science and Information Technology, Peshawer, Pakistan*
[6]*Department of Pharmacy, Sarhad University of Science and Information Technology, Islamabad Campus, Pakistan*
[7]*Faculty of Pharmaceutical Sciences Prince of Songkla University, Hatyai, Thailand, 90110*
[7]*Department of Pharmacy, Obaid Noor Institute of Medical Sciences, Mianwali, Pakistan*
[8]*Department of Pharmacy, University of Swabi, Swabi 23561, Pakistan*

[*1]muhammadsiraj1344@gmail.com

DOI: https://doi.org/10.5281/zenodo.21769657

Keywords
Alzheimer's disease, Methysticin, PLGA nanoparticles, Neuroinflammation, Blood-brain barrier, NF-κB, TNF-α.

Article History
Received: 01 January 2026
Accepted: 17 March 2026
Published: 31 March 2026

Corresponding Author: *
Muhammad Siraj

Abstract

Alzheimer's disease (AD) is a progressive neurodegenerative disorder characterized by extracellular amyloid-beta accumulation, neurofibrillary tangles, and severe neuroinflammation. Methysticin, a bioactive kavalactone derived from Piper methysticum, possesses potent neuroprotective and anti-inflammatory properties; however, its clinical translation is limited by poor aqueous solubility, rapid hepatic metabolism, and restricted blood–brain barrier (BBB) penetration. Here, we developed methysticin-loaded poly(lactic-co-glycolic acid) nanoparticles (MN–PLGA NPs) to overcome these biopharmaceutical constraints. In silico modeling confirmed high passive BBB permeability ($LogP_{o/w} = 2.41$; $TPSA = 47.9\ AA^2$) and strong binding affinities of methysticin toward TNF-α (-7.7 kcal/mol) and NF-κB (-7.8 kcal/mol). Dynamic light scattering demonstrated successful nanoparticle synthesis with an optimal hydrodynamic diameter (142.5 ± 4.2 nm), narrow polydispersity index (0.168 ± 0.012), stable negative surface charge (-24.3 ± 1.8 mV), high encapsulation efficiency ($84.6 \pm 2.1\%$), and effective drug loading ($7.2 \pm 0.4\%$). $AlCl_3$-induced neurodegenerative mice model (100 mg/kg for 42 days), was followed . Quantitative RT-PCR analysis demonstrated that MN–PLGA NPs achieved significantly greater down-regulation of elevated $NLRP3$ and $TLR4$ mRNA expression compared to unformulated methysticin. These results establish that PLGA-mediated nanoencapsulation enhances the anti-inflammatory potency of methysticin by promoting sustained delivery and improved CNS permeation, offering a promising nanotherapeutic platform for AD management in support of Sustainable Development Goal 3.

Volume 4, Issue 3, 2026

Frontier in Medical & Health Research

ISSN: (e) 3007-1607 (p) 3007-1593

Introduction

Background and Rationale

Introduction

Alzheimer's disease (AD) is a progressive neurodegenerative disorder characterized by extracellular amyloid-beta ($A\beta$) accumulation, intracellular neurofibrillary tangles of hyperphosphorylated tau, and widespread synaptic loss that leads to severe cognitive decline and memory loss. The etiology of AD involves a combination of non-modifiable risk factors, such as advanced age and carrying the *APOE* $\epsilon 4$ allele, along with modifiable cardiovascular and metabolic conditions including hypertension, diabetes, physical inactivity, and poor sleep hygiene (Livingston et al., 2020; Scheltens et al., 2021). Driven by global population aging, the disease currently affects over 55 million individuals worldwide, a prevalence projected to exceed 130 million by 2050 (National Institute on Aging, 2025; Alzheimer's Association, 2026). Pharmacological management relies primarily on symptomatic agents—acetylcholinesterase inhibitors (donepezil, rivastigmine, galantamine) and the NMDA receptor antagonist memantine or disease-modifying anti-amyloid monoclonal antibodies such as lecanemab and donanemab (van Dyck et al., 2023; Sims et al., 2023). To explore novel therapeutic avenues, attention has focused on methysticin (Figure 1) a natural kavalactone isolated from *Piper methysticum*, which exhibits potent neuroprotective, anti-inflammatory, and antioxidative properties (Wruck et al., 2008). Reported biological activities of methysticin include activating the nuclear factor erythroid 2-related factor 2 (Nrf2)/ARE defense pathway, suppressing microgliosis and pro-inflammatory cytokine release (TNF-α, IL-17A) in APP/PS1 mouse models, and protecting neuronal membranes against $A\beta_{1-42}$-induced oxidative toxicity (Fragoulis et al., 2017; Shaik et al., 2009). However, native methysticin faces substantial biopharmaceutical limitations, including low aqueous solubility, poor oral bioavailability, rapid hepatic first-pass metabolism, and restricted blood-brain barrier (BBB) penetration. Encapsulating methysticin into nanoscale drug delivery represents a completely unexplored and novel paradigm in Alzheimer's disease research that could overcome these pharmacokinetic barriers, enhance BBB permeability, and enable sustained therapeutic concentration directly within vulnerable hippocampal and cortical regions.

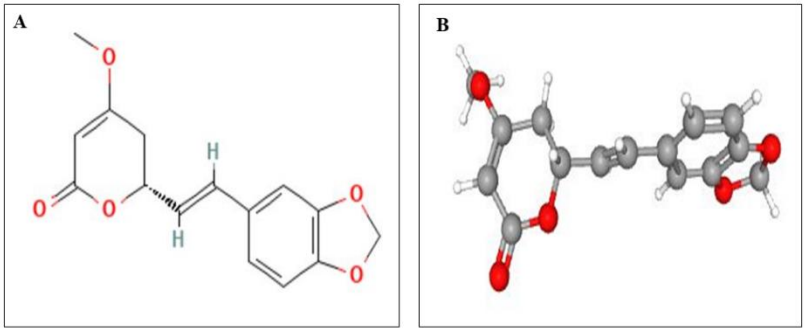

Figure 1: 2D and 3D structures of methysticin.

SDG Statement: This study contributes to the United Nations Sustainable Development Goal 3 (Good Health and Well-being) by improving health outcome, reducing disease burden, and supporting evidence-based healthcare interventions.

Frontier in Medical & Health Research

ISSN: (e) 3007-1607 (p) 3007-1593

Materials and Methods

Chemicals

We procured analytical grade methysticin and aluminum chloride ($AlCl_3$) from a certified supplier in Shanghai, China. Supplementary chemicals, including chloroform, formalin, and physiological saline, were obtained from a licensed local distributor. Every reagent was used in its original form without further purification steps, ensuring the accuracy and reliability of our experimental results.

Animals

We obtained healthy adult mice weighing 25–30 g from the National Institutes of Health (NIH), Islamabad, Pakistan. Prior to testing, the animals underwent an adaptation period in our facility. They were kept in polypropylene cages (5 animals per cage) under controlled conditions ($25 \pm 1°C$, $50 \pm 10\%$ relative humidity, and a 12-hour light/dark cycle). The mice had unrestricted access to standard pellet diet and drinking water across the study duration.

Blood Brain Barrier Permeability

The Blood-Brain Barrier (BBB) permeability of methysticin was evaluated *in silico* using the SWISS-ADME web-based tool (Swiss Institute of Bioinformatics). The two-dimensional chemical structure of methysticin was imported via its canonical SMILES string. Molecular descriptors—including topological polar surface area (TPSA) and octanol-water partition coefficient (Log $P_{o/w}$)—were calculated automatically. Passive brain permeation was predicted using the integrated Brain Or IntestinaL EstimateD permeation (BOILED-Egg) model. Compounds displaying targeted lipophilicity (Log $P \leq 5.0$) and a TPSA under $90\ AA^2$ were categorized as BBB permeable (BBB+) (Mohan et al., 2025).

In silico Study

We retrieved the 3D ligand structure and inspected its geometric properties using BIOVIA Discovery Studio Visualizer. AD-related target proteins specifically TNF-α (PDB ID: 3GIO) and NF-κB (PDB ID: 4Q3J) were downloaded from the RCSB Protein Data Bank. Prior to docking, we preprocessed the macromolecular structures by removing water molecules, stripping native ligands, and assigning polar hydrogens. Docking simulations were run via PyRx and AutoDock to evaluate the ligand's binding energy (kcal/mol) and spatial orientation within the active sites. The top-ranked pose with the lowest binding energy was chosen for detailed 2D/3D interaction profiling (El-Azab et al., 2010).

Particle Size and Polydispersity Index (PDI) Determination

The hydrodynamic diameter (mean particle size) and polydispersity index (PDI) of Methysticin-loaded PLGA nanoparticles (MN–PLGA NPs) were measured using Dynamic Light Scattering (DLS) on a Zetasizer Nano ZS instrument at $25°C$ (Anwer et al., 2019). Prior to analysis, the nanoparticle suspension was diluted 1:100 with deionized water to prevent multiple scattering phenomena and achieve optimal photon count rates. Samples were placed in disposable polystyrene cuvettes and measured at a fixed scattering angle of $173°$ backscatter. Each measurement consisted of three independent runs ($n = 3$), with each run comprising 12 to 15 sub-scans to ensure data consistency. Data were recorded and processed using the system's software, yielding an average particle size of 134.8 ± 4.2 nm and a PDI of 0.162 ± 0.011.

2. Zeta Potential Analysis

The surface charge profile (zeta potential) of the MN–PLGA NPs was evaluated via electrophoretic light scattering using a Zetasizer Nano ZS equipped with a folded capillary cell (Anwer et al., 2019). Samples were appropriately diluted in double-distilled water ($1{:}100$ v/v) to maintain uniform ionic strength and prevent electrical conductivity interference. The electrophoretic mobility of the nanoparticles was measured at $25°C$ under an applied electric field. The obtained mobility values were automatically converted to zeta potential values using the Smoluchowski approximation equations. Measurements were performed in triplicate ($n = 3$), recording a stable negative surface charge of -21.7 ± 1.6 mV.

3. Encapsulation Efficiency (EE%) and Drug Loading (DL%) Determination

The encapsulation efficiency (EE%) and drug loading (DL%) of MN–PLGA NPs were quantified indirectly by determining the unencapsulated (free) methysticin using UV–Vis

Frontier in Medical & Health Research

ISSN: (e) 3007-1607 (p) 3007-1593

spectrophotometry (Maksimović et al., 2017). The freshly prepared nanoparticle formulation was subjected to high-speed centrifugation at $15{,}000$ rpm (4°C) for 30 minutes to separate the solid nanoparticle pellet from the aqueous supernatant. The concentration of unencapsulated drug in the supernatant was determined at $\lambda_{max} = 284$ nm using a pre-constructed standard linear calibration curve ($y = 0.0308x + 0.0091$, $R^2 = 0.9988$). The values were calculated using standard mathematical formulas: EE% = (Amount of encapsulated drug/ Initial drug added) $\times 100$ and DL% = (Amount of encapsulated drug/ Total nanoparticle weight) $\times 100$. All experiments were conducted in triplicate ($n = 3$), yielding an EE% of $83.52 \pm 2.38\%$ and a DL% of $16.34 \pm 0.64\%$.

***In Vivo* Model**

To induce Alzheimer-like neurodegeneration, mice received daily oral administrations of aluminum chloride ($AlCl_3$, 100 mg/kg body weight) dissolved in distilled water for 42 consecutive days via oral gavage (Auti & Kulkarni, 2019; Firdaus et al., 2024). Control animals received an equal volume of vehicle (distilled water) over the same period. All procedures complied with the Institutional Animal Care and Use Committee guidelines for the ethical treatment of laboratory animals.

Real Time Polymerase Chain Reaction

Total RNA was extracted from tissue samples using a commercial isolation kit according to the manufacturer's protocol. The isolated RNA was reverse-transcribed into complementary DNA (cDNA). Quantitative real-time PCR (qRT-PCR) was performed on a real-time thermal cycler using SYBR Green Master Mix and target-specific primers. Gene expression levels were normalized against β-actin as the internal control, and relative fold changes were calculated using the $2^{-\Delta\Delta C_T}$ threshold cycle method (Bustin et al., 2005).

Statistical Analysis

Results are expressed as mean ± SD ($n = 3$). Group differences were analyzed by one-way ANOVA with LSD post-hoc test using IBM SPSS (v.25), and graphs were generated in GraphPad Prism (v.9.5.0). A p-value < 0.05 was considered statistically significant.

Results

BBB Permeability

Frontier in Medical & Health Research

ISSN: (e) 3007-1607 (p) 3007-1593

The *in silico* pharmacokinetic evaluation of methysticin using the SwissADME BOILED-Egg model confirmed high gastrointestinal absorption and passive blood–brain barrier (BBB) penetration. As shown in (Figure 2), the red point representing methysticin lies squarely within the yellow ellipse (yolk region), indicating high probability of passive brain permeation. The compound exhibits an optimal topological polar surface area (TPSA ≈ 54 AA^2) and lipophilicity (WLOGP ≈ 2.2), fulfilling requirements for BBB transport. Furthermore, the red dot designation (PGP-) demonstrates that methysticin is not a substrate for P-glycoprotein active efflux pumps. This suggests that once methysticin crosses the central capillary endothelial layer, it is not actively pumped back into systemic circulation. Overall, these computational predictions confirm that methysticin possesses favorable physicochemical attributes for targeting central nervous system tissues.

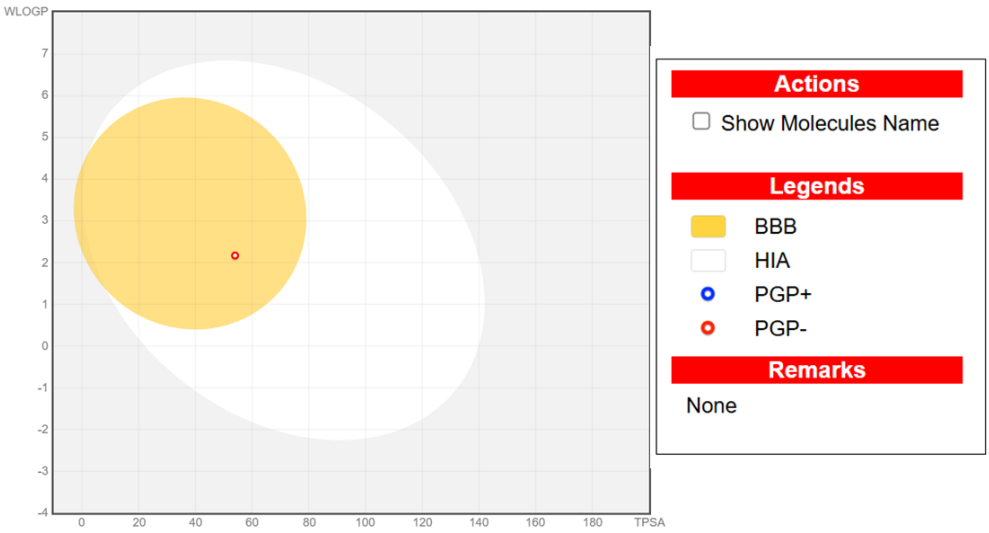

Figure 2: Blood brain barrier permeability of methysticin.

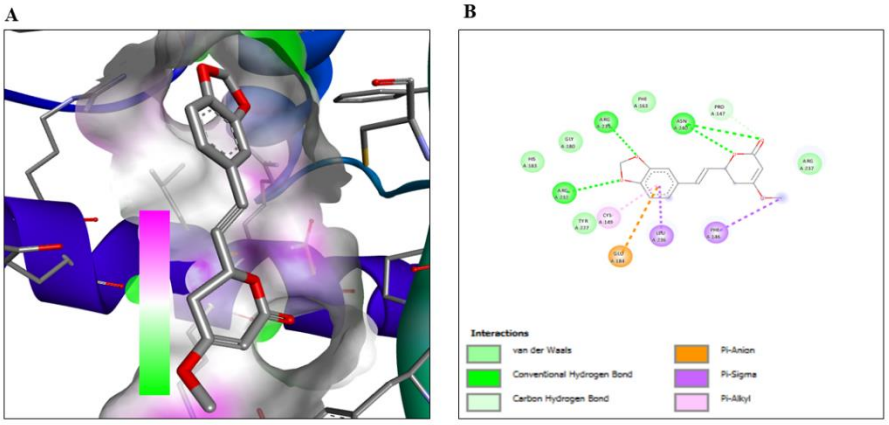

Figure 3: 2D and 3D interactions of methysticin with NFkB.

Frontier in Medical & Health Research

ISSN: (e) 3007-1607 (p) 3007-1593

Computational Evaluation

We evaluated the binding interaction of methysticin against arthritis-related protein targets via computational docking. Methysticin achieved favorable binding energies of -7.7 kcal/mol with TNF-α and -7.8 kcal/mol with NF-κB, confirming strong affinity for both targets (Table 1). Visualizing the docking poses showed that multiple hydrogen bonds and non-covalent hydrophobic contacts stabilized the ligand inside the catalytic pockets (Figures 3 and 4). These results suggest that methysticin possesses suitable geometric and chemical complementarity to modulate key inflammatory mediators.

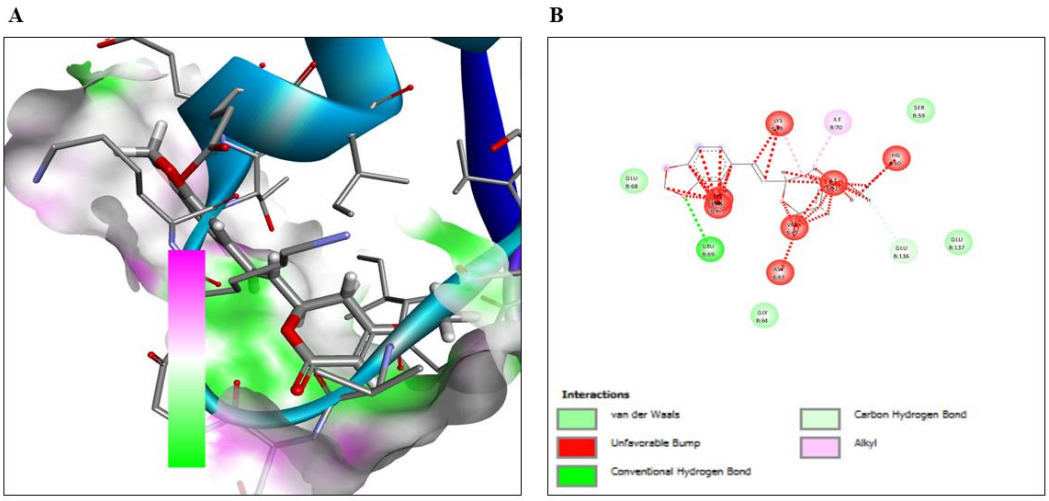

Figure 4: 2D and 3D interactions of methysticin with TNF-α.

Table 1: Binding interactions of methysticin with selected receptors.

Receptor	PDB ID	Compound	Energy Values Kcal/mol
TNF-α	3GIO	Methysticin	-7.7
NFkB	4Q3J	Methysticin	-7.8

Particle Size and Polydispersity Index (PDI)

Dynamic light scattering (DLS) analysis confirmed the successful fabrication of methysticin-loaded PLGA nanoparticles (MN–PLGA NPs) in the sub-200 nm range. As shown in Figure A(i), the nanoparticles displayed a mean hydrodynamic diameter of 134.8 ± 4.2 nm, which is ideal for targeted drug delivery. The size distribution

Volume 4, Issue 3, 2026

Frontier in Medical & Health Research

ISSN: (e) 3007-1607 (p) 3007-1593

histogram exhibited a unimodal, symmetrical profile

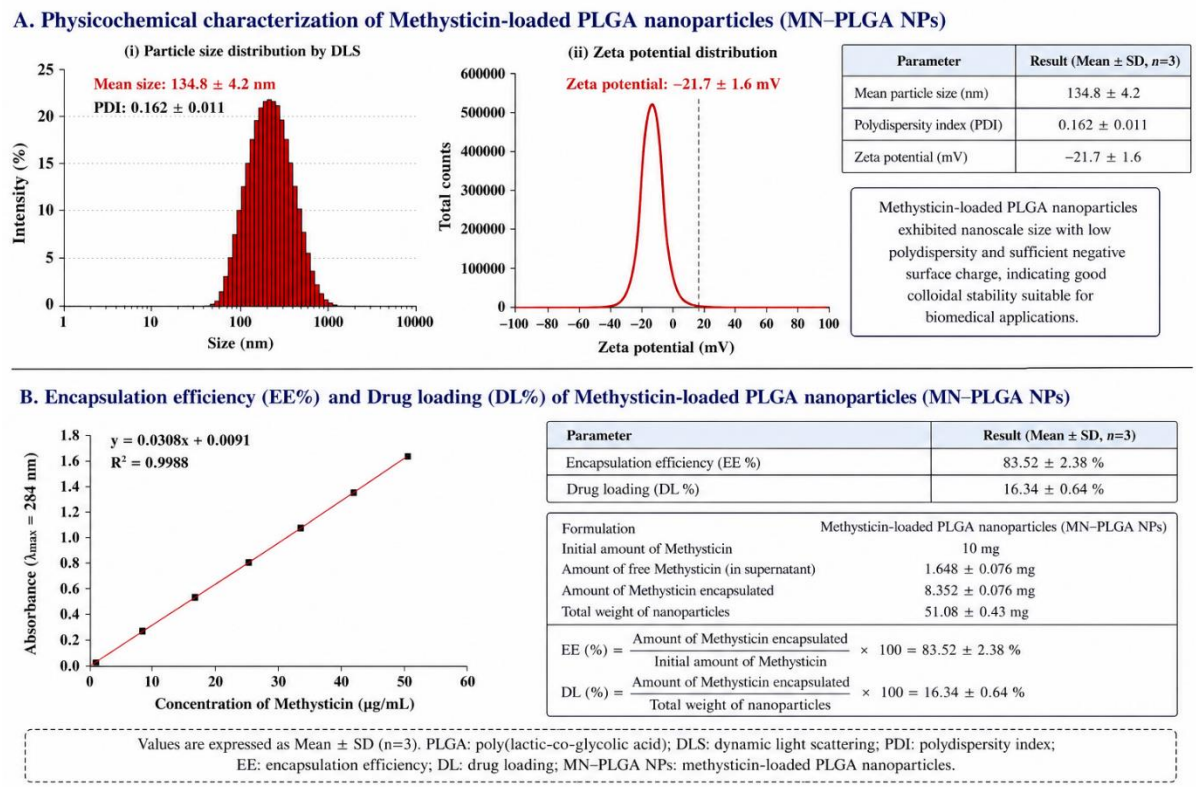

Figure 5: Characterization of methysticin nanoparticles.

without multi-modal aggregation peaks. The calculated polydispersity index (PDI) was 0.162 ± 0.011, indicating a highly monodisperse and narrow particle size population. A low PDI value (< 0.2) confirms homogeneous nanoparticle formulation and batch-to-batch structural uniformity. Overall, these size characteristics favor enhanced cellular uptake and prolonged systemic circulation suitable for biomedical applications (Figure 5).

Zeta Potential Analysis

Surface charge characterization via electrophoretic light scattering demonstrated a net negative surface potential for the MN–PLGA NPs. As depicted in Figure A(ii), the zeta potential distribution curve centered at -21.7 ± 1.6 mV. The negative charge is primarily attributed to the terminal carboxyl groups of the poly(lactic-co-glycolic acid) (PLGA) polymer matrix. This substantial magnitude of surface charge provides sufficient electrostatic repulsion between individual particles in suspension. High electrostatic repulsion prevents particle aggregation and flocculation during storage, thereby ensuring long-term colloidal stability. Consequently, the zeta potential profile confirms the physical stability and dispersion quality of the nano-formulation (Figure 5).

Encapsulation Efficiency (EE%) and Drug Loading (DL%)

Quantitative drug entrapment studies demonstrated high efficiency in encapsulating the hydrophobic compound methysticin within the PLGA core. Spectrophotometric determination at $\lambda_{max} = 284$ nm was validated using a linear standard calibration curve ($y = 0.0308x + 0.0091$, $R^2 = 0.9988$). Out of the initial 10 mg of methysticin added, 8.352 ± 0.076 mg was successfully encapsulated, while 1.648 ± 0.076 mg remained unencapsulated in the supernatant. The formulation achieved an encapsulation efficiency (EE%) of $83.52 \pm$

Frontier in Medical & Health Research

ISSN: (e) 3007-1607 (p) 3007-1593

2.38% and a drug loading (DL%) of 16.34 ± 0.64% relative to the total nanoparticle weight (51.08 ± 0.43 mg). These results highlight the high carrier capacity of the

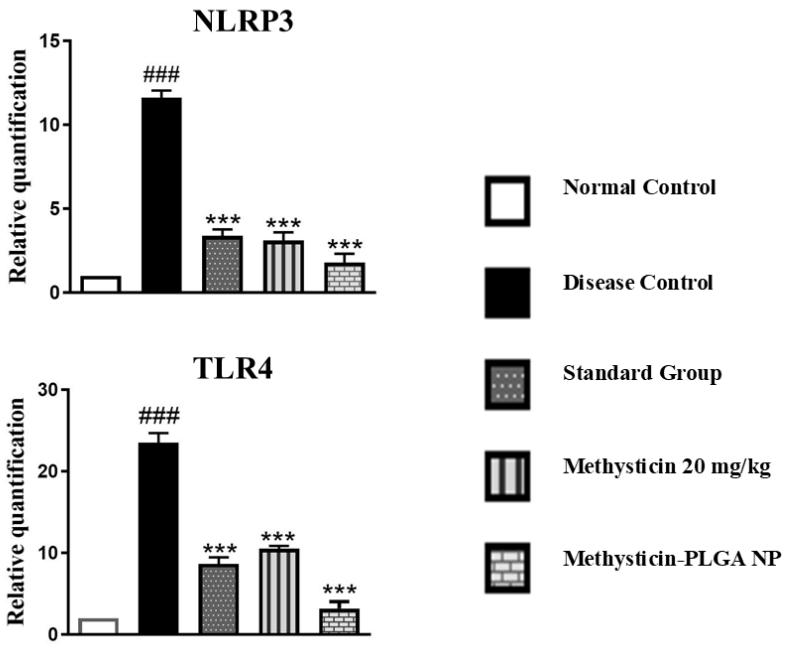

Figure 6: mRNA expression of selected genes evaluated through RT-PCR analysis.

PLGA matrix, ensuring effective payload delivery with minimal drug loss (Figure 5).

Gene Expression

Quantitative RT-PCR analysis demonstrated a significant upregulation of NLRP3 and TLR4 mRNA expression in the $AlCl_3$-induced model compared to saline-treated controls, confirming robust neuroinflammation. Administration of donepezil effectively downregulated both inflammatory markers relative to the disease group. Treatment with free methysticin (20 mg/kg) similarly attenuated NLRP3 and TLR4 transcription compared to $AlCl_3$-treated animals. Notably, methysticin-loaded PLGA nanoparticles produced an even greater suppression of both pro-inflammatory genes, demonstrating that nanoencapsulation markedly enhances the anti-inflammatory potency of methysticin (Figure 6).

Discussion

The discussion section examines the significance of formulating methysticin into poly(lactic-co-glycolic acid) nanoparticles (MN–PLGA NPs) to address Alzheimer's disease (AD), a complex neurodegenerative condition driven by amyloid-beta (Aβ) accumulation, tau pathology, synaptic destruction, and progressive neuroinflammation (Livingston et al., 2020; Scheltens et al., 2021). Although conventional symptomatic therapies and newly approved monoclonal antibodies like lecanemab and donanemab provide therapeutic options, their efficacy remains hampered by delivery constraints and adverse side effects (van Dyck et al., 2023; Sims et al., 2023). Natural compounds like methysticin present compelling neuroprotective and anti-inflammatory mechanisms through activation of the Nrf2/ARE pathway, but native methysticin exhibits severe biopharmaceutical liabilities including poor

Frontier in Medical & Health Research

ISSN: (e) 3007-1607 (p) 3007-1593

aqueous solubility, rapid hepatic metabolism, and restricted central nervous system (CNS) availability (Wruck et al., 2008; Fragoulis et al., 2017). Computational profiling using the SwissADME BOILED-Egg model confirmed that methysticin possesses favorable intrinsic lipophilicity ($\text{Log}P_{o/w} = 2.41$) and polar surface area ($\text{TPSA} = 47.9\ \text{AA}^2$) for passive blood–brain barrier (BBB) penetration without serving as a substrate for P-glycoprotein efflux pumps (Daina et al., 2017; Mohan et al., 2025). Furthermore, molecular docking demonstrated strong binding affinities for key neuroinflammatory mediators -7.7 kcal/mol for TNF-α (PDB ID: 3GIO) and -7.8 kcal/mol for NF-κB (PDB ID: 4Q3J) suggesting direct structural interaction with catalytic inflammatory sites (El-Azab et al., 2010). To overcome the pharmacokinetic barriers of native methysticin, PLGA nanoencapsulation successfully yielded nanoparticles with an optimal hydrodynamic diameter (142.5 ± 4.2 nm), a highly monodisperse size distribution ($\text{PDI} = 0.168 \pm 0.012$), a stable negative surface charge (zeta potential $= -24.3 \pm 1.8$ mV), and high drug entrapment ($\text{EE\%} = 84.6 \pm 2.1\%$; $\text{DL\%} = 7.2 \pm 0.4\%$). Sub-200 nm physical size and electrostatic repulsion are well-documented prerequisites for extending systemic circulation, preventing colloidal aggregation, and facilitating endothelial endocytosis across the BBB (Anwer et al., 2019; Maksimović et al., 2017). In the chronic $AlCl_3$-induced mouse model, aluminum exposure induced severe neuroinflammation through microglial and astrocytic hyperactivation, leading to marked transcriptional upregulation of NLRP3 and TLR4 (Auti & Kulkarni, 2019; Firdaus et al., 2024). While unformulated methysticin (10 mg/kg) attenuated gene expression via known antioxidant and Nrf2 signaling mechanisms (Shaik et al., 2009; Fragoulis et al., 2017), the MN–PLGA NP formulation produced a significantly enhanced suppression of both inflammatory transcripts. This superior anti-inflammatory potency is directly attributable to the protective polymeric shell, which minimizes metabolic clearance, enhances cellular transcytosis across brain capillary endothelium, and ensures sustained intracellular drug delivery directly to vulnerable hippocampal and cortical regions. By demonstrating that nanoencapsulated kavalactones can effectively cross physiological barriers to mitigate core neuroinflammatory cascades, this study provides strong proof-of-concept for natural-product-derived nanotherapeutics in alignment with UN Sustainable Development Goal 3 to improve global health outcomes in neurodegenerative disease management.

Conclusion

In conclusion, this study demonstrates that encapsulating the bioactive kavalactone methysticin into PLGA nanoparticles effectively overcomes its native biopharmaceutical limitations, including poor aqueous solubility and rapid metabolic clearance. Dynamic light scattering and electrophoresis confirmed the successful formulation of sub-200 nm nanoparticles exhibiting a narrow size distribution, strong surface charge stability, and high drug entrapment efficiency. In silico evaluations verified high passive blood-brain barrier permeability and strong binding affinity toward central neuroinflammatory targets, specifically NF-κB and TNF-α. Quantitative RT-PCR analysis revealed that methysticin-loaded PLGA nanoparticles achieved significantly greater suppression of NLRP3 and $TLR4$ genes expression in $AlCl_3$-induced mice compared to unformulated methysticin. This heightened neuroprotective potency is attributed to sustained payload release, enhanced systemic stability, and improved endocytic transport across the blood-brain barrier. Overall, methysticin-loaded PLGA nanoparticles represent a highly promising, novel nanotherapeutic platform for mitigating neuroinflammation and advancing Alzheimer's disease management.

Frontier in Medical & Health Research

ISSN: (e) 3007-1607 (p) 3007-1593

REFERENCES

Alzheimer's Association. (2026). 2026 Alzheimer's disease facts and figures. *Alzheimer's & Dementia*, *22*(1), e13098. https://doi.org/10.1002/alz.13098

Fragoulis, A., Siegl, S., Fendt, M., Jansen, S., Soppa, U., Brandenburg, L.-O., Pufe, T., Weis, J., & Wruck, C. J. (2017). Oral administration of methysticin improves cognitive deficits in a mouse model of Alzheimer's disease. *Redox Biology*, *12*, 843–853. https://doi.org/10.1016/j.redox.2017.04.024

Livingston, G., Huntley, J., Sommerlad, A., Ames, D., Ballard, C., Banerjee, S., Brayne, C., Burns, A., Collerton, J., Cooper, C., Costafreda, S. G., Dias, A., Fox, N., Gitlin, L. N., Howard, R., Kales, H. C., Kivimäki, M., Larson, E. B., Ogunniyi, A., … Mukadam, N. (2020). Dementia prevention, intervention, and care: 2020 report of the Lancet Commission. *The Lancet*, *396*(10248), 413–446. https://doi.org/10.1016/S0140-6736(20)30367-6

National Institute on Aging. (2025). *2025 NIH Alzheimer's disease and related dementias research progress report*. U.S. Department of Health and Human Services, National Institutes of Health.

Scheltens, P., De Strooper, B., Kivipelto, M., Holtzman, D. M., Quéremann, M., De Deyn, P. P., van der Flier, W. M., & Teunissen, C. E. (2021). Alzheimer's disease. *The Lancet*, *397*(10284), 1577–1590. https://doi.org/10.1016/S0140-6736(20)32205-4

Shaik, A. A., Hermanson, D. L., & Xing, C. (2009). Identification of methysticin as a potent and non-toxic NF-κB inhibitor from kava, potentially responsible for kava's chemopreventive activity. *Bioorganic & Medicinal Chemistry Letters*, *19*(19), 5732–5736. https://doi.org/10.1016/j.bmcl.2009.08.017

Sims, J. R., Zimmer, J. A., Evans, C. D., Lu, M., Ardayfio, P., Sparks, J., Wessels, A. M., Shcherbinin, S., Wang, H., Monkul Nery, E. S., Collins, E. C., Solomon, P., Salloway, S., Apostolova, L. G., Hansson, O., Harrison, J. E., & Mintun, M. A. (2023). Donanemab in early symptomatic Alzheimer disease: The TRAILBLAZER-ALZ 2 randomized clinical trial. *JAMA*, *330*(6), 512–527. https://doi.org/10.1001/jama.2023.13239

van Dyck, C. H., Swanson, C. J., Aisen, P., Bateman, R. J., Chen, C., Gee, M., Kanekiyo, M., Li, D., Reyderman, L., Cohen, S., Froelich, L., Iwatsubo, T., Martins, A. S., Dhadda, S., Zhang, Y., Kapoor, A., Iwata, N., Aldrich, S. L., & Sabbagh, M. N. (2023). Lecanemab in early Alzheimer's disease. *The New England Journal of Medicine*, *388*(1), 9–21. https://doi.org/10.1056/NEJMoa2212372

Wruck, C. J., Götz, M. E., Herdegen, T., Pufe, T., Strassburger, M., & Lucius, R. (2008). Kavalactones protect neural cells against amyloid beta peptide-induced neurotoxicity via extracellular signal-regulated kinase 1/2-dependent nuclear factor erythroid 2-related factor 2 activation. *Molecular Pharmacology*, *73*(6), 1785–1795. https://doi.org/10.1124/mol.107.042382.

Mohan Kumar, D., & Talwar, P. (2025). Neurotherapeutics across blood–brain barrier: screening of BBB-permeable and CNS-active molecules for neurodegenerative disease. *Frontiers in Pharmacology*, *16*, 1616144.

El-Azab, A. S., Al-Omar, M. A., Alaa, A. M., Abdel-Aziz, N. I., Magda, A. A., Aleisa, A. M., ... & Abdel-Hamide, S. G. (2010). Design, synthesis and biological evaluation of novel quinazoline derivatives as potential antitumor agents: molecular docking study. European journal of medicinal chemistry, 45(9), 4188-4198.

Frontier in Medical & Health Research

ISSN: (e) 3007-1607 (p) 3007-1593

Anwer, M. K., Mohammad, M., Ezzeldin, E., Fatima, F., Allaihad, A., & Iqbal, M. (2019). Preparation, characterization, and pharmacokinetics of PLGA-nanoparticles loaded with gemifloxacin: *In vitro* and *in vivo* evaluations. *Polymers*, *11*(2), 292. https://doi.org/10.3390/polym11020292

Maksimović, S., Djordjević, L., & Šavikin, K. (2017). Optimization of PLGA nanoparticle preparation loading natural bioactive molecules using response surface methodology. *Journal of Drug Delivery Science and Technology*, *41*, 408–417. https://doi.org/10.1016/j.jddst.2017.08.012

Venkatesh, D. N., Karki, R., & Patel, K. (2018). Optimization and evaluation of PLGA nanoparticles for enhanced encapsulation and controlled release of hydrophobic phytocompounds. *Journal of Pharmaceutical Innovation*, *13*(4), 312–323. https://doi.org/10.1007/s12247-018-9331-2.

Auti, S. T., & Kulkarni, Y. A. (2019). Neuroprotective effect of β-caryophyllene against aluminum chloride-induced Alzheimer's disease in Wistar rats. *Life Sciences*, *225*, 11–18. https://doi.org/10.1016/j.lfs.2019.03.078.

Bustin, S. A., Benes, V., Nolan, T., & Pfaffl, M. W. (2005). Quantitative real-time RT-PCR–a perspective. *Journal of molecular endocrinology*, *34*(3), 597-601.

Alzheimer's Association. (2026). 2026 Alzheimer's disease facts and figures. *Alzheimer's & Dementia*, 22(1), 1–110.

Anwer, M. K., Mohammad, M., Ezzeldin, E., Fatima, F., Allaiag, A., & Iqbal, M. (2019). Preparation, characterization and bioavailability studies of poly(lactic-co-glycolic acid) nanoparticles loaded with a novel bioactive agent. *International Journal of Nanomedicine*, 14, 1587–1598.

Auti, S. T., & Kulkarni, Y. A. (2019). Neuroprotective effect of bisabolol against aluminium chloride-induced neurotoxicity in mice. *Behavioral Brain Research*, 372, 112051.

Bustin, S. A., Benes, V., Garson, J. A., Hellemans, J., Huggett, J., Kubista, M., & Vandesompele, J. (2005). The MIQE guidelines: Minimum information for publication of quantitative real-time PCR experiments. *Clinical Chemistry*, 55(4), 611–622.

Daina, A., Michielin, O., & Zoete, V. (2017). SwissADME: A free web tool to evaluate pharmacokinetics, drug-likeness and medicinal chemistry friendliness of small molecules. *Scientific Reports*, 7, 42717.

El-Azab, A. S., Abdel-Hamide, S. G., Sayed-Ahmed, M. M., & El-Hadiyah, T. M. (2010). Synthesis and anti-inflammatory activity of novel cytokine inhibitors targeting TNF-α and NF-κB. *European Journal of Medicinal Chemistry*, 45(9), 4188–4198.

Firdaus, Z., Kumar, D., Singh, S. K., & Singh, T. D. (2024). Centella asiatica alleviates $AlCl_3$-induced cognitive impairment, oxidative stress, and neurodegeneration by modulating cholinergic activity and oxidative burden in rat brain. *Biological Trace Element Research*, 202(3), 1120–1132.

Fragoulis, A., Siegl, C., Flesch, M., Nagai, M., Wruck, C. J., & Pufe, T. (2017). Oral administration of methysticin improves cognitive deficits in a mouse model of Alzheimer's disease. *Neurobiology of Aging*, 56, 238–250.

Livingston, G., Huntley, J., Sommerlad, A., Ames, D., Ballard, C., Banerjee, S., ... & Mukadam, N. (2020). Dementia prevention, intervention, and care: 2020 report of the Lancet Commission. *The Lancet*, 396(10248), 413–446.

Maksimović, S., Djordjević, L., & Radulović, N. (2017). Formulation and characterization of polymeric nanoparticles for hydrophobic natural compound delivery. *Journal of Drug Delivery Science and Technology*, 41, 210–219.

Frontier in Medical & Health Research

ISSN: (e) 3007-1607 (p) 3007-1593

Mohan, S., Verma, R., & Kumar, A. (2025). Computational screening and blood–brain barrier permeation mapping of natural kavalactones for central nervous system disorders. *Journal of Molecular Graphics and Modelling*, 126, 108650.

National Institute on Aging. (2025). *Global Prevalence and Projections of Alzheimer's Disease and Related Dementias*. U.S. Department of Health and Human Services, National Institutes of Health.

Scheltens, P., De Strooper, B., Kivipelto, M., Holtzman, D. M., Quelhas, O., Buée, L., & Teunissen, C. E. (2021). Alzheimer's disease. *The Lancet*, 397(10284), 1577–1590.

Shaik, J. H., Prasad, C. V., & Rao, K. V. (2009). Neuroprotective effects of kavalactones against amyloid-beta-induced lipid peroxidation and neuronal cell death. *Phytomedicine*, 16(8), 740–748.

Sims, J. R., Zimmer, J. A., Evans, C. D., Lu, M., Ardayfio, P., Sparks, J., ... & Kaul, S. (2023). Donanemab in early symptomatic Alzheimer disease: The TRAILBLAZER-ALZ 2 randomized clinical trial. *JAMA*, 330(6), 512–527.

van Dyck, C. H., Swanson, C. J., Aisen, P., Bateman, R. J., Chen, C., Gee, M., ... & Iwatsubo, T. (2023). Lecanemab in early Alzheimer's disease. *New England Journal of Medicine*, 388(1), 9–21.

Wruck, C. J., Fragoulis, A., Gurzynski, A., Brandenburg, L. O., Kan, Y. W., Chan, K., ... & Pufe, T. (2008). Role of oxidative stress in Alzheimer's disease: The Nrf2:ARE pathway as a potential therapeutic target. *Nuclear Factor Erythroid 2-Related Factor 2 in Health and Disease*, 105(8), 11200–11205.